JACS Au
AN OPEN ACCESS JOURNAL OF THE AMERICAN CHEMICAL SOCIETY

pubs.acs.org/jacsau
Article

Construction of Compartmentalized Meso/Micro Spaces in Hierarchically Porous MOFs with Long-Chain Functional Ligands Inspired by Biological Signal Amplification

Yao Tong, Jian Yang, Fan Xia, and Jinlou Gu*

Cite This: JACS Au 2025, 5, 178−186
Read Online

ACCESS | Metrics & More | Article Recommendations | Supporting Information

ABSTRACT: The creation of spatially coupled meso-/micro-environments with biomimetic compartmentalized functionalities is of great significance to achieve efficient signal transduction and amplification. Herein, using a soft-template strategy, UiO-67-type hierarchically mesoporous metal−organic frameworks (HMMOFs) were constructed to satisfy the requirements of such an artificial system. The key to the successful synthesis of HMUiO-67 is rooted in the utilization of the preformed cerium-oxo clusters as metal precursors, aligning the growth of MOF crystals with the mild conditions required for the self-assembly of the soft template. The adoption of long-chain functional 2,2′-bipyridine-5,5′-dicarboxylic acid ligands not only resulted in larger microporous sizes, facilitating the transport of various cascade reaction intermediates, but also provided anchorages for the introduction of enzyme-mimicking active sites. A cascade amplification system was designed based on the developed HMUiO-67, in which enzyme cascade reactions were initiated and relayed by a target analyte in the separate but coupled meso/micro spaces. As a proof of concept, natural acetylcholinesterase (AChE) and Cu-based laccase mimetics were integrated into HMMOFs, establishing a spatially coupled nanoreactor. The activity of AChE was triggered by the target analyte of carbaryl, while the amplified products of AChE catalysis mediated the activity of biomimetic enzyme in the closely proximate microporous spaces, producing further amplification of detectable signal. This enabled the entire cascade system to respond to minimal carbaryl with a limit of detection as low as approximately 2 nM. Such a model of cascade amplification is expected to set a conceptual guideline for the rational design of various bioreactors, serving as a sensitive response system for quantifying numerous target analytes.

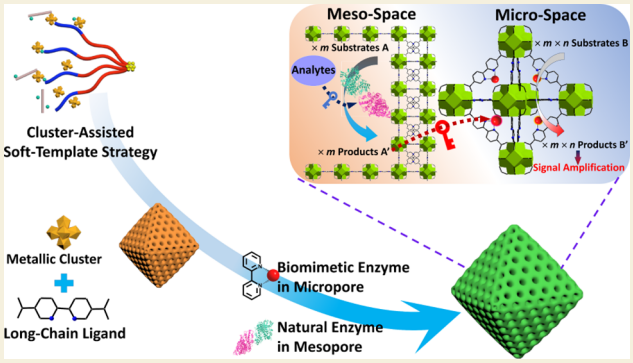

KEYWORDS: *metallic clusters, template synthesis, hierarchically mesoporous MOFs, biomimetic reaction, signal amplification*

INTRODUCTION

Through long-term natural selection, biological compartmentalization and cascade reaction therein have evolved into the optimal pathway to achieve efficient intracellular signal transduction and amplification.[1−3] Confined intracellular compartments enable a highly coupled and ordered spatial arrangement of multistep biological reactions while separating them from harmful external interferences.[4] This compartmentalization allows even a very small amount of intermediate products to act as potent activators for the following reaction in the cascade. As a result, the system is highly sensitive to minimal input signals, allowing it to recognize and respond to substrates at extremely low levels.[5,6] Such an orchestrated amplification mechanism might provide inspiration for building separate but coupled meso-/microenvironments, laying the principle for the design of an efficient synthetic reactor based on porous materials.[7−13]

Hierarchically mesoporous MOFs (HMMOFs) could satisfy the prerequisites of such artificial systems.[14−26] They not only inherit the advantages of traditional microporous crystalline MOFs, such as inherent high porosity and variable composition, but also bear abundant size-tunable mesopores for large-molecule accommodation while still retaining sufficient space for the free diffusion of reactants.[27−31] Especially, when using the soft template as a structure-directing agent, the introduced uniform mesopores within HMMOFs are seamlessly surrounded by micropores, facilitating the shuttle and communication of reaction intermediates between meso/micro spaces.[32] Through mimicking the organization characteristic of biological compartmentalization,

Received: September 18, 2024
Revised: December 19, 2024
Accepted: December 20, 2024
Published: December 31, 2024

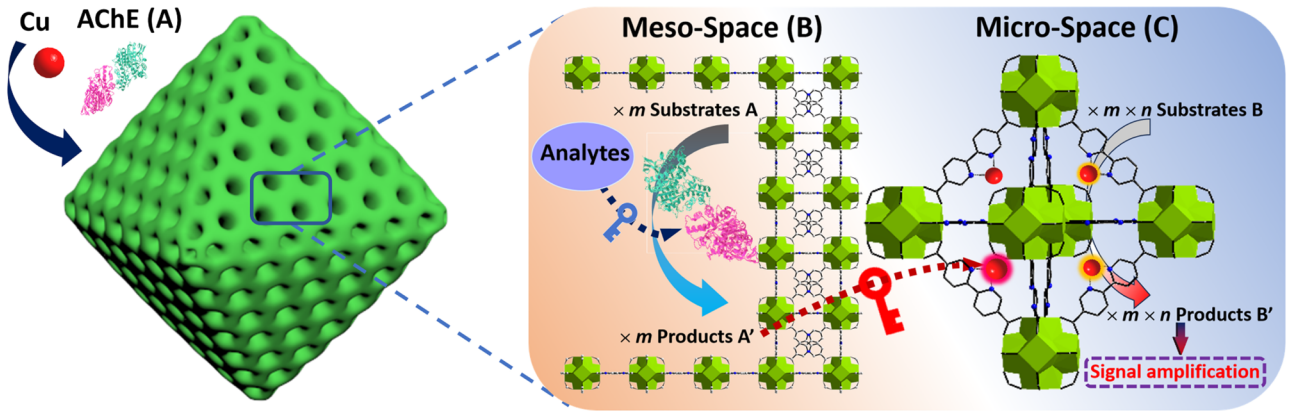

Figure 1. Schematic illustration of the compartmentalized meso/micro spaces in the designed HMUiO-67-Cu. (A) Natural AChE was encapsulated in mesopore, while Cu-based biomimetic enzyme was introduced in micropore of HMMOFs. Signal amplification through cascade reaction between (B) natural enzyme in mesoporous space and (C) biomimetic enzyme in microporous space.

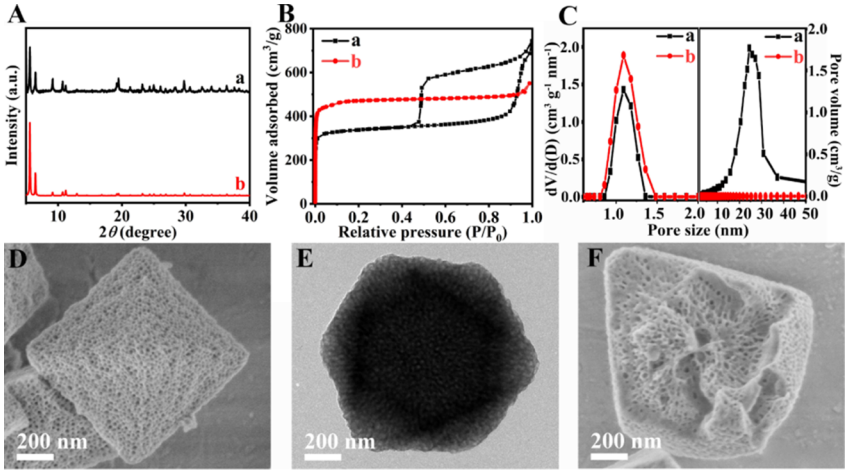

Figure 2. (A) XRD patterns, (B) N_2 sorption isotherms, and (C) their corresponding pore size distribution of the as-synthesized HMUiO-67 (a) and simulated microporous counterpart (b). (D) SEM, (E) TEM, and (F) typical fracture surface SEM images of the as-synthesized HMUiO-67.

the synergetic work of different guest molecules spatially separated in the neighboring mesoporous and microporous domains can be achieved. Unfortunately, the reported soft-template-directed HMMOFs were usually constructed with organic ligands of short-chain terephthalic acid or its derivatives so that their mesoporous wall typically possessed a micropore of approximately 0.6 to 0.8 nm in size.[33,34] The small microporous reaction spaces generally restrict the effective diffusion of many types of intermediates between adjacent functional pore units, affecting the overall signal communication efficiency of the simulated compartments.[35,36] Therefore, constructing HMMOFs with longer ligands to afford larger micropores and their enhanced accessibility to the reaction intermediates is of great significance for achieving a more efficient biomimetic compartmentalized cascade reaction.

The conventional synthesis of MOFs with long-chain ligands typically employs metal ions as precursors, which need to first form ordered metal clusters before they are organized into a crystalline structure. This process requires overcoming significant energy barriers and is usually carried out under relatively harsh conditions such as at high temperatures.[37,38] Such a stringent requirement for MOF growth is generally incompatible with the mild environment needed for soft-template-directed self-assembly. Ongoing studies have verified that the utilization of preformed metallic clusters as precursors in microporous MOF synthesis could effectively reduce the reaction temperature and avoid harsh conditions.[39−41] Such advancement of cluster-assisted synthesis prompts us to explore the direct construction of HMMOFs using the preformed metallic cluster subunit to overcome the thermodynamic dilemma of MOF crystallization and micellar assembly. Herein, the preformed octahedral Ce_6-oxo clusters were adopted to build hierarchically mesoporous Ce-based MOFs (HMUiO-67) under mild aqueous conditions, using long-chain functional 2,2′-bipyridine-5,5′-dicarboxylic acid (BPyDC) as a linker to address the limitations of UiO-66-type HMMOFs. The utilization of BPyDC as a ligand results in larger microporous sizes, facilitating the transport of various cascade reaction intermediates. Additionally, the BPyDC ligand also provides anchorages through its nitrogen atoms in bipyridine moieties, which can be conveniently functionalized to introduce numerous biomimetic active sites.[42,43]

To validate the model of the biomimetic compartmentalized cascade amplification based on the obtained HMMOFs, a natural enzyme was encapsulated in the mesoporous domain, while long-chain functional ligands in the microporous domain were modified as biomimetic enzymes, resulting in a larger microporous space with more accessible active sites (Figure 1A). The activity of natural enzymes could be triggered by the external stimulus (Figure 1B), while the products generated by

https://doi.org/10.1021/jacsau.4c00866
JACS Au 2025, 5, 178−186

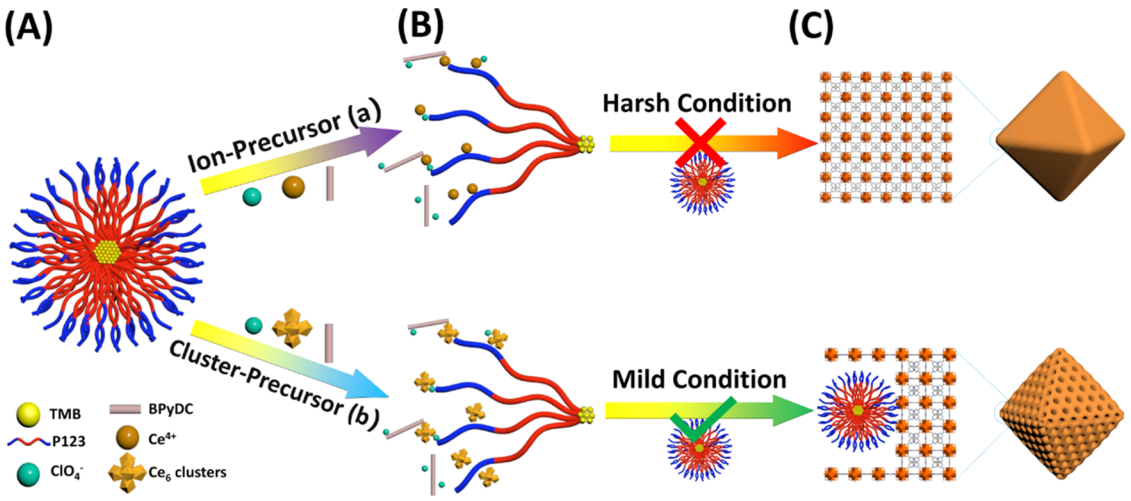

Figure 3. Schematic illustration for the failed (a) and successful (b) soft-template-directed synthesis of HMUiO-67 with long-chain functional BPyDC as organic ligands as well as Ce^{4+} and the preformed Ce_6 clusters as metallic precursors, respectively.

enzymatic-catalysis amplification in the mesoporous domain would mediate the activity of the biomimetic enzyme in the closely proximate micropore, producing further amplified detectable signals (Figure 1C). To exemplify such a concept, we focused on the sensitive detection of carbaryl, a representative carbamate pesticide known for causing neurological toxicity even at extremely low concentrations.[44] Natural AChE and the biomimetic enzyme of Bpy-Cu were integrated into HMMOFs, creating a spatially coupled nanoreactor. AChE catalyzed the hydrolysis of acetylthiocholine (ATCh) to a thiol-containing product (thiocholine, TCh), while its catalytic activity could be sensitively inhibited by a carbaryl. Bpy-Cu has been confirmed to feature efficient laccase-like activity, which could be regulated by reductive TCh since such activity was closely relevant to the valence state of Cu species.[45,46] Trace amounts of carbaryl could give rise to the change in AChE activity, while the catalytic products of TCh acted as activators for the coupled chromogenic reaction catalyzed by the biomimetic enzyme in microporous space. This enabled the entire cascade system to respond to minimal carbaryl with a limit of detection (LOD) as low as approximately 2 nM. Such a concept of cascade amplification could be simply extended by altering the types of natural or biomimetic enzymes, hopefully setting a guideline for the rational design of multiple response systems to quantify multifarious enzymatic inhibitors or promoters.

RESULTS AND DISCUSSION

By substituting the preformed cerium-oxo clusters for Ce^{4+} as the metal precursor, UiO-67-type HMMOFs constructed with long-chain functional BPyDC ligands were obtained using a soft-template strategy.[47] The peaks in the wide-angle X-ray diffraction (XRD) pattern of HMUiO-67 matched well with those of the simulated UiO-67 counterpart, confirming the formation of the crystalline framework (Figure 2A).[48] The abundant micropores rationalized the steep rise in the N_2 sorption isotherm at low relative pressure from 0 to 0.04. The large H2-type hysteresis loop at a relative pressure of about 0.45 evidenced the presence of cage-type mesopores (Figure 2B). The micropore diameter was calculated to be approximately 1.1 nm by density functional theory (DFT) (Figure 2C, left panel), while the mesopore diameter was determined to be about 24.5 nm using the Barrett−Joyner−Halenda (BJH) model with the adsorption branch (Figure 2C, right panel). Scanning electron microscopy (SEM) images indicated that HMUiO-67 consisted of regular octahedron particles with a remarkably uniform arrangement of mesopores on their surface (Figure 2D). Transmission electron microscopy (TEM) and a typical SEM image of the fracture surface further revealed the formation of cage-type mesostructures throughout the whole particle of HMMOFs (Figure 2E,F). The IR bands at 1600 and 1410 cm^{-1} could be assigned to the asymmetric and symmetric stretching vibration of O−C−O of the BPyDC linkers in HMUiO-67 after its coordination with Ce_6 clusters.[48] Simultaneously, the FT-IR spectra depicted the disappearance of ν(C═O) bands at 1690 cm^{-1} of acetic acid and free BPyDC, ν(C−H) bands at 2880 cm^{-1} and ν(C−O−C) bands at 1120 cm^{-1} of surfactant templates, verifies the successful removal of the modulator, free ligands, and surfactant after adequate ethanol extraction (Figure S1).[23] Thermogravimetric analysis (TGA) indicated that the as-synthesized HMUiO-67 could endure heat treatment at high temperatures up to 300 °C, consistent with the reported excellent thermal stability of its microporous counterpart.[48] Meanwhile, the number of linker deficiencies per Ce_6 formula unit was calculated to be about 1.35 based on the TGA data, which implies that the molar ratio of metal (Ce)/ligand (BPyDC) is approximately 1.35:1 (Figure S2).[49]

To gain insight into the formation mechanism of HMUiO-67, a series of control experiments were performed. As a structure-directing agent, P123 is expected to guide the self-assembly of MOF precursors into a mesostructure with the assistance of ClO_4^-.[20] In the first step, the Pluronic copolymer and aromatic agent tended to aggregate in aqueous solution and form spherical-like micelles with 1,3,5-trimethylbenzene (TMB) and the PPO block as hydrophobic inner cores surrounded by hydrophilic PEO coronas at the periphery (Figure 3A).[22,50] As a swelling agent, TMB would expand the radius of the P123 micelle and correspondingly regulate the mesopore size of HMMOFs. Along with the increase of the TMB/P123 feed ratio, the mesopore diameters were enlarged from 13 to 28 nm (Figures S3−S5).[22] Since the multivalent metal species would coordinate with PEO segments of micelles to form crown-ether-type complexes, the periphery of the

https://doi.org/10.1021/jacsau.4c00866
JACS Au 2025, 5, 178−186

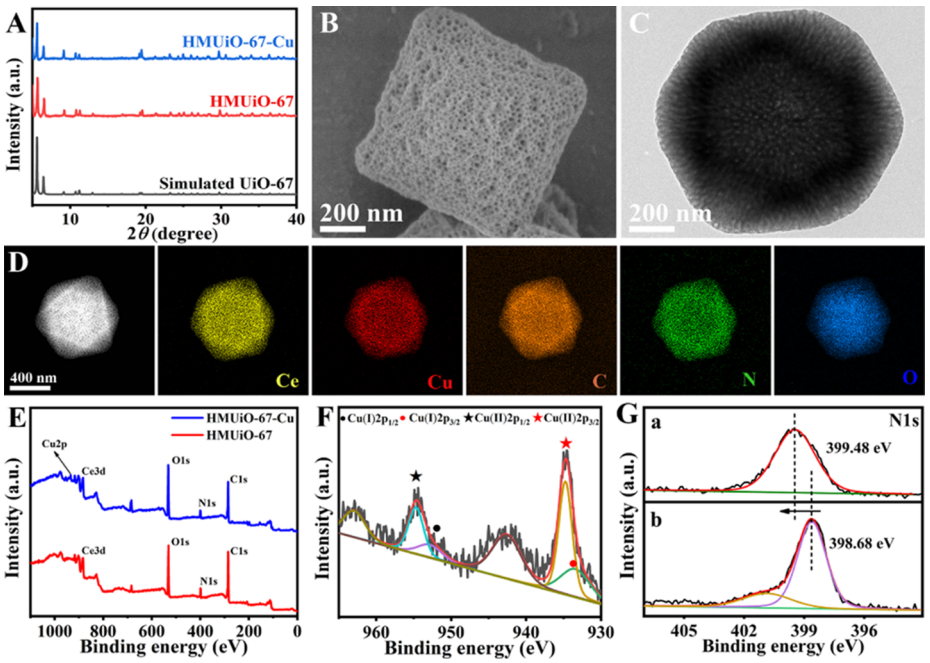

Figure 4. (A) XRD patterns of the as-synthesized HMUiO-67-Cu (blue), HMUiO-67 (red), as well as the simulated microporous UiO-67 counterpart. (B) SEM, (C) TEM, and (D) the corresponding element mappings of Ce, Cu, C, N, and O in the as-synthesized HMUiO-67-Cu. (E) Wide-scan and the corresponding (F) Cu 2p and (G) N 1s XPS of HMUiO-67 after (a) and before (b) the introduction of Cu species.

spherical micelles would be surrounded by Ce-oxo clusters or Ce^{4+} ions. It has been well documented that Hofmeister salting-in ions of ClO_4^- are readily polarized and present a high affinity toward the hydrophobic BPyDC ligands. The accumulation of ClO_4^- around BPyDC would attract and bridge Ce_6 nodes, promoting the growth of the crystallized MOFs around the templates (Figure 3B).[51] The control experiments showed that when the ClO_4^-/Ce feed ratio was less than 8, the products lacked crystallinity and a mesoporous structure. The crystalline HMUiO-67 obviously evolved when the ClO_4^-/Ce feed ratios were set between 8.7 and 11. Further increasing the ClO_4^-/Ce feed ratio beyond 13.2, the overly strong interaction between ClO_4^- and metal precursors inhibited the growth of crystals, resulting in the formation of mesopores without crystalline pore walls (Figures S6 and S7).[22]

The key to the successful synthesis of HMUiO-67 stems from the substitution of the preformed Ce_6 clusters for Ce^{4+} as metallic precursors. Conventional Ce-UiO-67 built from metal ions and organic ligands were typically synthesized by the solvothermal method.[49] However, the harsh conditions involving excess organic solvent and high temperatures extremely restrict the self-assembly of amphiphilic surfactant, which generally proceeds under a mild aqueous environment. The control experiments also indicated that the product synthesized directly using Ce^{4+} ions at 40 °C not only presented poor crystallinity but also lacked a mesoporous structure since the traditional synthesis of Ce-UiO-67 typically occurred at 100 °C (Figures S8 and S9). Recent consensus has been reached that the adoption of the preformed metal-oxo clusters as metallic sources could effectively reduce the reaction temperature and avoid harsh reaction conditions.[52,53] The glycinate/nitrate-capped Ce_6-oxo clusters could be easily obtained in water and maintained excellent stability under experimental conditions, as verified by XRD patterns (Figures S10 and S11).[47] Benefiting from the direct coordination between Ce_6-oxo clusters and BPyDC ligands, the energy consumption was significantly reduced, ensuring that the reaction was capable of proceeding at a relatively low temperature. Such a mild aqueous environment guaranteed the spontaneous formation of Pluronic copolymer micelles to direct the growth of HMMOFs (Figure 3C). It is worth noting that the utilization of the preformed clusters also reduced the dosage of modulator required for the synthesis of HMUiO-67. As a modulator, acetic acid (HAc) could compete with linkers to control the rates of crystal growth.[54] However, a precise trace amount of HAc (HAc/Ce feed ratio, 0.3:1) was enough to promote the formation of well-crystallized products (Figures S12 and S13), while excessive modulator (HAc/Ce feed ratio, 0.5:1) would intensely inhibit the reaction process and dramatically reduce the yield.

In virtue of the competence of N-heterocycle in BPyDC ligands to coordinate with various metal ions, the Cu^{2+} could be facilely introduced in situ into the microporous domain of HMUiO-67, endowing it with laccase-like properties.[46,55] The integrities of the crystalline structure and morphology of HMUiO-67 were well preserved during such functionalization (Figure 4A,B). The mesostructure remained practically unchanged, as evidenced by the hysteresis loop in the N_2 sorption isotherm and the corresponding mesopore size distribution in line with the observation of TEM (Figure 4C). Obvious reductions in microporous surface area and micropore size consumedly correlated with the fact that Cu species were located in the microporous spaces (Figure S14 and Table S1). The homogeneous distribution of Ce, Cu, C, N, and O elements in the as-synthesized HMUiO-67-Cu was verified by the elemental mappings in concert with the expected coordination of Cu and nitrogen in BPyDC (Figure 4D). The Ce/Cu molar ratio was approximately 1.3:1, as determined by inductively coupled plasma optical emission spectrometry. Combined with the result derived from the TGA profile (Figure S2), the molar ratio of Cu/BPyDC could be

https://doi.org/10.1021/jacsau.4c00866
JACS Au 2025, 5, 178−186

confirmed as nearly 1:1. Such virtually equivalent amounts of Cu species and BPyDC proved that Cu occupied almost all the N-sites of the ligands.[48,56]

To directly explore the coordination environment and valence state of the Cu species, X-ray photoelectron spectroscopy (XPS) was recorded on the samples before and after the introduction of Cu active centers. The wide-scan XPS spectra displayed a new weak peak corresponding to Cu species after functionalization (Figure 4E). The coexistence of Cu^{+} and Cu^{2+} in the Cu 2p spectrum manifested the transfer of electrons from N atoms in pyridine to Cu^{2+}, further confirming the occurrence of Cu−N chelation (Figure 4F). The peak of N 1s XPS (about 398.68 eV) shifted toward the higher energy direction (about 399.48 eV) in correlation to the decrease in the electron cloud density of N atoms resulting from the ligand-to-metal charge transfer (Figure 4G).[56] Such coordination between copper ions and the N atoms in the abundant bipyridine moieties of the organic ligands clearly verified the successful introduction of biomimetic laccase-like Bpy-Cu active sites into the microdomains of HMUiO-67 in agreement with our proposal.

The laccase-mimicking catalytic activity of HMUiO-67-Cu was confirmed by its competence to catalyze the chromogenic reaction between 2,4-dichlorophenol (2,4-DP) and 4-pyridinamine (4-AP), resulting in a bright red color and a strong absorption at 510 nm in accordance with natural laccase (Figure 5A).[57] As expected, the kinetic parameters of the

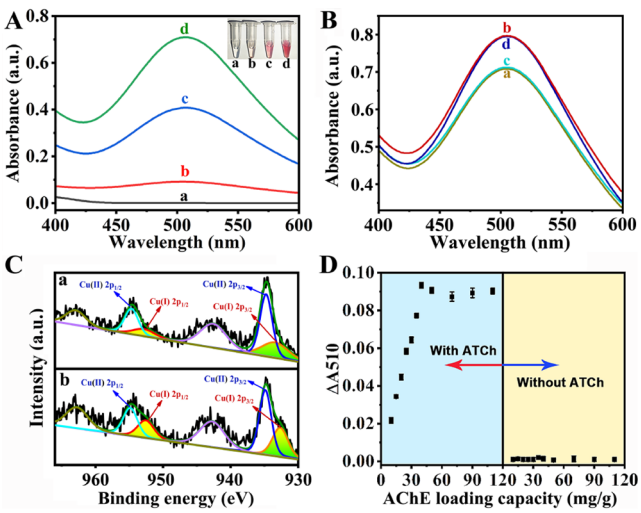

Figure 5. (A) UV−visible absorption spectra of 2,4-DP/4-AP solution (a) in the presence of HMUiO-67 (b), natural laccase (c), and HMUiO-67-Cu (d). The inset demonstrates the corresponding digital photographs. (B) UV−visible absorption spectra of HMUiO-67-Cu sensing system in the presence of 2,4-DP/4-AP (a), AChE and ATCh (b), HAc (c), as well as TCh (d). (C) High-resolution Cu 2p XPS spectra of HMUiO-67-Cu before (a) and after (b) incubation with the AChE and ATCh. (D) Relationship between ΔA510 of the developed response system and AChE loading capacity in the presence (blue) and absence (yellow) of ATCh.

chromogenic reaction catalyzed by HMUiO-67-Cu conformed to the Michaelis−Menten equation (Figure S15). The important parameters of the Michaelis−Menten constant (K_m) and maximum initial velocity (V_{max}) were calculated by Lineweaver−Burk plots. The open mesoporous channels in HMUiO-67-Cu provide sufficient space for the substrates to diffuse and transfer toward uniformly distributed Cu sites. Additionally, the confinement effect of the microporous structure facilitates the proximity of substrates to enzymes, also benefiting to a smaller K_m value than many reported copper-containing nanozymes (Table S2).[58,59] Such a stronger affinity between HMUiO-67-Cu and substrates would enhance its catalytic efficiency.

To construct a compartmentalized cascade amplification system, the immobilization of AChE in mesopores is crucial for the rapid conversion of substrates to mediate the activity of the biomimetic enzyme in the coupled micropores. The maximum AChE loading capacity of HMUiO-67-Cu was quantified to be about 248 mg/g (Figure S16). The crystalline octahedral morphology and open mesoporous channels of parent HMUiO-67-Cu were well preserved, as evidenced by SEM and TEM observations, indicating that the encapsulation of AChE would not destroy its structural integrity (Figure S17). Meanwhile, the N_2 sorption isotherm and its corresponding mesopore size distribution revealed the sharp reduction of the mesoporosity after enzyme loading, corroborating the successful entrapment of AChE within the mesopores rather than the external surface (Figure S18 and Table S3). The leaching degree of AChE was also traced, which revealed that only a small amount of AChE leaked from the applied HMUiO-67-Cu after its soaking in Tris-HCl buffer for even up to 24 h, indicative of its successful immobilization within mesopores (Figure S19). Since the three-dimensional parameters of AChE (4.5 nm × 6.0 nm × 6.5 nm) are far smaller than the mesopore size, there still exists enough space for the free diffusion of substrates and the procession of the enzymatic reaction.[60]

To verify the critical activation effect of TCh on the laccase-like catalytic activity of BPy-Cu in HMUiO-67-Cu, we conducted a series of control experiments using several molecules as promoters for a biomimetic enzyme. During experiments, we found that the crystalline stability of HMUiO-67 was perfectly maintained in buffer solution and testing conditions despite that the trace amount of Ce^{4+} was reduced to Ce^{3+}, which posed negligible influence on the sensing properties of the probe (Figures S20 and S21). Upon the addition of AChE or its substrate ATCh alone to the reactor, a negligible change of the catalytic activity was observed (Figure S21). In contrast, when both AChE and ATCh were simultaneously added, the catalytic activity of HMUiO-67-Cu significantly increased, as evidenced by the greatly enhanced absorbance at 510 nm (Figure 5B, curve b). This suggested that the catalytic product of TCh might really serve as a promoter for the biomimetic enzyme of BPy-Cu. Given that AChE catalyzed ATCh to produce both HAc and TCh, we compared the effects of these products on the catalytic activity of HMUiO-67-Cu. No alteration of catalytic activity was observed in the presence of HAc (Figure 5B, curve c), whereas only 20 nM TCh significantly enhanced the laccase-like activity of HMUiO-67-Cu (Figure 5B, curve d), clearly supporting the fact that TCh did play a signal relay role between micro/mesopore units. The enhancement mechanism of the catalytic activity was explored by XPS analysis. The peaks at 933.8 and 953.2 eV, corresponding to Cu^{+}, remarkably elevated after incubating HMUiO-67 with TCh, indicating the reduction of Cu^{2+} to Cu^{+} by TCh (Figure 5C). The increased proportion of Cu^{+}/Cu^{2+} is generally responsible for the higher laccase-mimicking activity of HMUiO-67-Cu.[45] These results demonstrated that trace amounts of TCh were crucial for activating the coupled cascade reaction in microporous spaces. Such an

https://doi.org/10.1021/jacsau.4c00866
JACS Au 2025, 5, 178−186

activation effect is highly beneficial for constructing a sensitive cascade-triggered response system, as even slight changes in enzymatic activity in the mesoporous spaces can lead to the variation of TCh activator levels, which would be greatly amplified in the coupled reaction occurring in the microporous spaces.

To balance the activation efficiency for the biomimetic enzyme and high sensitivity toward the analyte detection, it is necessary to precisely control the amount of the immobilized AChE in HMUiO-67-Cu. First, we optimized the working parameters for the entire response system, including the concentration of ATCh substrate, pH, reaction time, as well as reaction temperature, in order to make the chromogenic reaction catalyzed by the biomimetic enzyme function effectively (Figure S22). Under the optimized conditions, as the AChE loading capacities increased from 0 to 40 mg/g, the activation effect toward the biomimetic enzyme gradually enhanced and finally reached its maximum (Figures 5D and S23A). Further increasing the AChE loading capacities from 40 to 120 mg/g did not improve the activation effect, as almost all Cu active sites in the coupled microporous spaces were activated by TCh and retained in equilibrium. Additionally, higher AChE loading would require more inhibitor to suppress its catalytic activity, which is detrimental to maintaining high sensitivity. On the other hand, in the absence of ATCh, the absorbance of the response system remained almost unchanged regardless of the loading amount of AChE, further confirming the role of the catalytic product TCh in signal transduction between porous units of different sizes (Figure 5D, right panel).

To explore the application potentials of the elaborated cascade amplification system, we chose a typical carbaryl pesticide as a detection target to evaluate its sensing performance. In the human body, a trace amount of carbaryl could effectively inhibit the activity of AChE so that the normal breakdown of acetylcholine is prevented in the nervous system, leading to the accumulation of acetylcholine at nerve synapses. This accumulation triggers a cascade of amplified physiological reactions, ultimately disrupting nerve signal transmission. Inspired by such natural systems, we aimed to design an efficient biomimetic response system to sensitively detect carbaryls using the resultant AChE@HMUiO-67-Cu. The inhibition of the AChE activity by carbaryl would hinder the production of TCh, resulting in a reduced enhancement of the laccase-like activity of HMUiO-67-Cu. The enzyme loading quantity of HMUiO-67-Cu is crucial for ensuring a sufficient activation effect while maintaining high sensitivity. Thus, we compared two response systems with optimal (40 mg/g) and relatively low (20 mg/g) AChE loading capacities, respectively. With the continuous introduction of carbaryl, the absorbances of both response systems gradually weakened, which coincided with the reduction in TCh activator levels and the corresponding decrease of biomimetic enzyme activity in the microporous spaces (Figure S23B). As shown in Figure 6A, |ΔA510|, the absolute value of the absorbance difference at 510 nm of the response systems in the absence and presence of carbaryl, gradually enhanced with the increase of carbaryl concentration, resulting from the progressive decrease of AChE activity in the mesopore. Poor linear correlation between absorbance and logarithm of the carbaryl concentration was presented for the response system with lower AChE loading capacity (20 mg/g) since insufficient enzymes in the mesoporous spaces are prone to be saturated by the

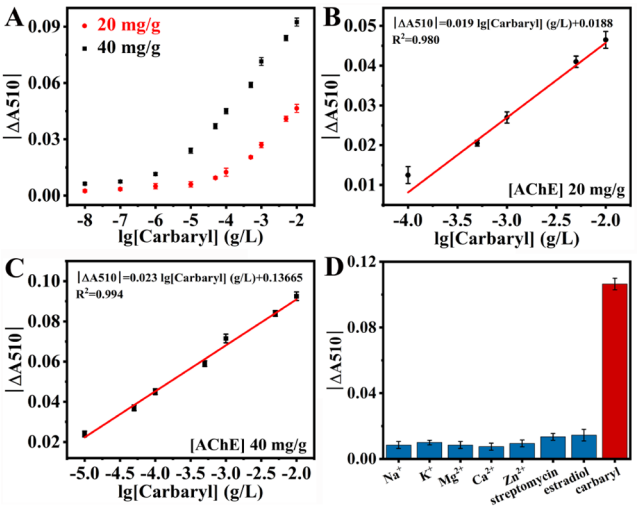

Figure 6. (A) Relationship between |ΔA510| and logarithm of the carbaryl concentration for HMUiO-67-Cu with AChE loading capacities of 20 mg/g (red) and 40 mg/g (black). Linear fitting curves between |ΔA510| and the logarithm of the carbaryl concentration for the cascade amplification system of HMUiO-67-Cu with AChE loading capacities of 20 mg/g (B) and 40 mg/g (C). (D) Anti-interference tests with the developed response platform for the specific carbaryl (50 nM) detection in the presence of a range of possibly coexistent metal ions (100 μM), streptomycin (10 μM) and estradiol (10 μM).

substrates (Figure 6B). Comparatively, HMUiO-67 with an AChE loading capacity of 40 mg/g featured a wider linear detection range ($1 \times 10^{-5} \sim 1 \times 10^{-2}$ g/L) and a good linear correlation with the logarithm of the carbaryl concentration with a coefficient constant (R^2) of 0.994 (Figure 6C). Based on the 3σ rule, the LOD was determined to be as low as 2 nM, exhibiting a higher sensitivity than several reported models (Table S4). Such unique sensing properties toward carbaryl were almost unaffected by possibly coexistent interfering species including metal ions, estradiol, and antibiotics (Figure 6D). The practical ability of the developed cascade amplification system for the carbaryl detection was evaluated by spiking carbaryl to local real water. As depicted in Table S5, satisfactory recoveries (98.4−100.4%) and RSD (1.75−4.98%) were achieved, prefiguring a promising prospect for practical applications of the developed compartmentalized cascade amplification system.

CONCLUSIONS

In summary, using a soft-template strategy, UiO-67-type HMMOFs were constructed. The utilization of the preformed metallic clusters enabled the assembly of long-chain functional ligands into HMUiO-67, which not only resulted in larger microporous sizes, ensuring the efficient mass exchange between the different pore units, but also provided anchorages for the introduction of active sites. Natural AChE and laccase-like BPy-Cu were spatially positioned into the separate meso/micro spaces, respectively, forming a cascade signal amplification system, in which the intermediates produced from mesoporous domains mediated the activity of biomimetic enzymes in the closely proximate microporous spaces. The signal amplification in such a compartmentalized bioreactor enabled it to respond to extremely small amounts of the model target analyte of carbaryl with an LOD as low as approximately 2 nM. Such a concept of cascade amplification could be simply

https://doi.org/10.1021/jacsau.4c00866
JACS Au 2025, 5, 178−186

extended by altering the types of natural or biomimetic enzymes in meso/micro spaces separately, hopefully setting a guideline for the rational design of multiple response systems to quantify multifarious target analytes.

■ ASSOCIATED CONTENT

Supporting Information

The Supporting Information is available free of charge at https://pubs.acs.org/doi/10.1021/jacsau.4c00866.

Experimental details, XRD patterns, TGA curves, FTIR spectra, BET profiles, SEM and TEM images, and UV−vis spectra (Tables S1−S5) (PDF)

■ AUTHOR INFORMATION

Corresponding Author

Jinlou Gu − *Key Lab for Ultrafine Materials of Ministry of Education, School of Materials Science and Engineering, East China University of Science and Technology, Shanghai 200237, China;* orcid.org/0000-0002-3190-573X; Email: jinlougu@ecust.edu.cn

Authors

Yao Tong − *Key Lab for Ultrafine Materials of Ministry of Education, School of Materials Science and Engineering, East China University of Science and Technology, Shanghai 200237, China*

Jian Yang − *Key Lab for Ultrafine Materials of Ministry of Education, School of Materials Science and Engineering, East China University of Science and Technology, Shanghai 200237, China;* orcid.org/0000-0002-4451-0497

Fan Xia − *Key Lab for Ultrafine Materials of Ministry of Education, School of Materials Science and Engineering, East China University of Science and Technology, Shanghai 200237, China*

Complete contact information is available at: https://pubs.acs.org/10.1021/jacsau.4c00866

Author Contributions

The manuscript was written through the contributions of all authors. All authors have approved the final version of the manuscript.

Notes

The authors declare no competing financial interest.

■ ACKNOWLEDGMENTS

This work was financially supported by the Natural Science Foundation of China (22275054, 52103314, 21975072, and 51902106), the Program of Shanghai Academic Research Leader (23XD1401000), and the Chenguang Plan of Shanghai Education Development Foundation (21CGA38).

■ REFERENCES

(1) Bar-Peled, L.; Kory, N. Principles and Functions of Metabolic Compartmentalization. *Nat. Metab.* **2022**, *4*, 1232−1244.

(2) Carceller, J. M.; Arias, K. S.; Climent, M. J.; Iborra, S.; Corma, A. One-Pot Chemo- and Photo-Enzymatic Linear Cascade Processes. *Chem. Soc. Rev.* **2024**, *53*, 7875−7938.

(3) Hooe, S. L.; Smith, A. D.; Dean, S. N.; Breger, J. C.; Ellis, G. A.; Medintz, I. L. Multienzymatic Cascades and Nanomaterial Scaffolding—A Potential Way Forward for the Efficient Biosynthesis of Novel Chemical Products. *Adv. Mater.* **2024**, *36* (5), 2309963.

(4) Kröll, S.; Niemeyer, C. M. Nucleic Acid-Based Enzyme Cascades-Current Trends and Future Perspectives. *Angew. Chem., Int. Ed.* **2024**, *63*, No. e202314452.

(5) Rabe, K. S.; Müller, J.; Skoupi, M.; Niemeyer, C. M. Cascades in Compartments: En Route to Machine-Assisted Biotechnology. *Angew. Chem. Int. Ed.* **2017**, *56* (44), 13574−13589.

(6) Bowness, J. M. Epinephrine: Cascade Reactions and Glycogenolytic Effect. *Science* **1966**, *152*, 1370−1371.

(7) Wang, Y.; Zhao, Q.; Haag, R.; Wu, C. Biocatalytic Synthesis Using Self-Assembled Polymeric Nano- and Microreactors. *Angew. Chem. Int. Ed.* **2022**, *61* (52), No. e202213974.

(8) Li, Z.; Xu, K.; Qin, L.; Zhao, D.; Yang, N.; Wang, D.; Yang, Y. Hollow Nanomaterials in Advanced Drug Delivery Systems: From Single- to Multiple Shells. *Adv. Mater.* **2023**, *35*, 2203890.

(9) Wang, R.; Yu, Y.; Gai, M.; Mateos-Maroto, A.; Morsbach, S.; Xia, X.; He, M.; Fan, J.; Peng, X.; Landfester, K.; Jiang, S.; Sun, W. Liposomal Enzyme Nanoreactors Based on Nanoconfinement for Efficient Antitumor Therapy. *Angew. Chem. Int. Ed.* **2023**, *62* (44), No. e202308761.

(10) Feng, J.; Duan, J.; Hung, C.-T.; Zhang, Z.; Li, K.; Ai, Y.; Yang, C.; Zhao, Y.; Yu, Z.; Zhang, Y.; Wang, L.; Zhao, D.; Li, W. Micelles Cascade Assembly to Tandem Porous Catalyst for Waste Plastics Upcycling. *Angew. Chem. Int. Ed.* **2024**, *63* (26), No. e202405252.

(11) Gao, R.; Kou, X.; Tong, L.; Li, Z.-W.; Shen, Y.; He, R.; Guo, L.; Wang, H.; Ma, X.; Huang, S. M.; Chen, G.; Ouyang, G. Ionic Liquid-Mediated Dynamic Polymerization for Facile Aqueous-Phase Synthesis of Enzyme-Covalent Organic Framework Biocatalysts. *Angew. Chem. Int. Ed.* **2024**, *63* (8), No. e202319876.

(12) Xu, H.; Han, J.; Zhao, B.; Sun, R.; Zhong, G.; Chen, G.; Yamauchi, Y.; Guan, B. A facile dual-template-directed successive assembly approach to hollow multi-shell mesoporous metal−organic framework particles. *Nat. Commun.* **2023**, *14* (1), 8062.

(13) Jiang, S.; da Silva, L. C.; Ivanov, T.; Mottola, M.; Landfester, K. Synthetic Silica Nano-Organelles for Regulation of Cascade Reactions in Multi-Compartmentalized Systems. *Angew. Chem. Int. Ed.* **2022**, *61* (6), No. e202113784.

(14) Cai, G. R.; Yan, P.; Zhang, L. L.; Zhou, H.-C.; Jiang, H.-L. Metal-Organic Framework-Based Hierarchically Porous MaterialsSynthesis and Applications. *Chem. Rev.* **2021**, *121*, 12278−12326.

(15) Li, J.; Li, R.; Wang, W.; Lan, K.; Zhao, D. Ordered Mesoporous Crystalline Frameworks Toward Promising Energy Applications. *Adv. Mater.* **2024**, *36* (16), 2311460.

(16) Yao, Y.; Zhao, X.; Chang, G.; Yang, X.; Chen, B. Hierarchically Porous Metal-Organic Frameworks: Synthetic Strategies and Applications. *Small Struct.* **2023**, *4* (9), 2200187.

(17) Wen, S. L.; Fu, Q. J.; Yan, L. T.; Zhao, X. B. Hierarchically Porous Three-Dimensional-Ordered Macro-Microporous Metal Organic Frameworks: Design, Precise Synthesis, and Applications. *Coord. Chem. Rev.* **2024**, *517*, 215996.

(18) Dutta, S.; Kumari, N.; Dubbu, S.; Jang, S. W.; Kumar, A.; Ohtsu, H.; Kim, J.; Cho, S. H.; Kawano, M.; Lee, I. S. Highly Mesoporous Metal-Organic Frameworks as Synergistic Multimodal Catalytic Platforms for Divergent Cascade Reactions. *Angew. Chem. Int. Ed.* **2020**, *59*, 3416−3422.

(19) Zhang, X. L.; Tu, R. X.; Lu, Z.; Peng, J. Y.; Hou, C. T.; Wang, Z. H. Hierarchical Mesoporous Metal-Organic Frameworks Encapsulated Enzymes: Progress and Perspective. *Coord. Chem. Rev.* **2021**, *443*, 214032.

(20) Li, K.; Yang, J.; Huang, R.; Lin, S. L.; Gu, J. L. Ordered Large-Pore MesoMOFs Based on Synergistic Effects of Triblock Polymer and Hofmeister Ion. *Angew. Chem. Int. Ed.* **2020**, *59*, 14124−14128.

(21) Zhao, L. W.; Yang, J.; Gong, M.; Li, K.; Gu, J. L. Specific Screening of Prostate Cancer Individuals Using an Enzyme-Assisted Substrate Sensing Platform Based on Hierarchical MOFs with Tunable Mesopore Size. *J. Am. Chem. Soc.* **2021**, *143*, 15145−15151.

(22) Li, K.; Zhao, Y.; Yang, J.; Gu, J. Nanoemulsion-Directed Growth of MOFs with Versatile Architectures for the Heterogeneous Regeneration of Coenzymes. *Nat. Commun.* **2022**, *13* (1), 1879.

(23) Yang, J.; Gong, M.; Xia, F.; Tong, Y.; Gu, J. Hofmeister Effect Promoted the Introduction of Tunable Large Mesopores in MOFs at Low Temperature for Femtomolar ALP Detection. *Adv. Sci.* **2024**, *11* (4), 2305786.
(24) Zhao, Y. J.; Zhu, L. Y.; Tang, J.; Fu, L.; Jiang, D.; Wei, X. Q.; Nara, H.; Asahi, T.; Yamauchi, Y. Enhancing Electrocatalytic Performance via Thickness-Tuned Hollow N-Doped Mesoporous Carbon with Embedded Co Nanoparticles for Oxygen Reduction Reaction. *ACS Nano* **2024**, *18*, 373−382.
(25) Zhao, Y. J.; Zhu, L. Y.; Kang, Y. Q.; Shen, C. H.; Liu, X. Y.; Jiang, D.; Fu, L.; Guselnikova, O.; Huang, L. J.; Song, X. K.; Asahi, T.; Yamauchi, Y. Nanoengineering Multilength-Scale Porous Hierarchy in Mesoporous Metal-Organic Framework Single Crystals. *ACS Nano* **2024**, *18*, 22404−22414.
(26) Li, X.; Wu, X.-T.; Xu, Q.; Zhu, Q.-L. Hierarchically Ordered Pore Engineering of Metal−Organic Framework-Based Materials for Electrocatalysis. *Adv. Mater.* **2024**, *36* (27), 2401926.
(27) Wang, X. W.; Ma, T.; Ma, J.-G.; Cheng, P. Integration of Devices Based on Metal-Organic Frameworks: A Promising Platform for Chemical Sensing. *Coord. Chem. Rev.* **2024**, *518*, 216067.
(28) Zhang, J.; Jin, N.; Chen, X.; Shen, Y.; Pan, T.; Li, L.; Li, S.; Zhang, W.; Huo, F. The Encounter of Biomolecules in Metal-Organic Framework Micro/Nano Reactors. *ACS Appl. Mater. Interfaces* **2021**, *13*, 52215−52233.
(29) Wei, Y. Z.; Feng, J. Y.; Guan, B. Y.; Yu, J. H. Structural Engineering of Hierarchical Zeolite-Based Catalysts. *Acc. Chem. Res.* **2024**, *5*, 857−871.
(30) Tian, G.; Chen, G. R.; Yang, G. J.; Diao, Z. H.; Bai, R. S.; Han, J.; Guan, B. Y.; Yu, J. H. Construction of Metal/Zeolite Hybrid Nanoframe Reactors via in-Situ-Kinetics Transformations. *ACS Cent. Sci.* **2024**, *10*, 1473−1480.
(31) Liang, J. Y.; Gao, S.; Liu, J.; Zulkifli, M. Y. B.; Xu, J. T.; Scott, J.; Chen, V.; Shi, J. F.; Rawal, A.; Liang, K. Hierarchically Porous Biocatalytic MOF Microreactor as a Versatile Platform Towards Enhanced Multienzyme and Cofactor-Dependent Biocatalysis. *Angew. Chem. Int. Ed.* **2021**, *60*, 5421−5428.
(32) Li, K.; Yang, J.; Gu, J. Hierarchically Porous MOFs Synthesized by Soft-Template Strategies. *Acc. Chem. Res.* **2022**, *55*, 2235−2247.
(33) Cavka, J. H.; Jakobsen, S.; Olsbye, U.; Guillou, N.; Lamberti, C.; Bordiga, S.; Lillerud, K. P. A New Zirconium Inorganic Building Brick Forming Metal Organic Frameworks with Exceptional Stability. *J. Am. Chem. Soc.* **2008**, *130* (42), 13850−13851.
(34) You, Q.; Wang, H.; Zhao, Y.; Fan, W. T.; Gu, W. M.; Jiang, H.-L.; Wu, Z. K. Bottom-Up Construction of Metal-Organic Framework Loricae on Metal Nanoclusters with Consecutive Single Nonmetal Atom Tuning for Tailored Catalysis. *J. Am. Chem. Soc.* **2024**, *146*, 9026−9035.
(35) Akpinar, I.; Wang, X. L.; Fahy, K.; Sha, F. R.; Yang, S. L.; Kwon, T.-W.; Das, P. J.; Islamoglu, T.; Farha, O. K.; Stoddart, J. F. Biomimetic Mineralization of Large Enzymes Utilizing a Stable Zirconium-Based Metal-Organic Frameworks. *J. Am. Chem. Soc.* **2024**, *146*, 5108−5117.
(36) Han, J.; Xu, H. D.; Zhao, B.; Sun, R. G.; Chen, G. R.; Wu, T. Y.; Zhong, G. Y.; Gao, Y. J.; Zhang, S. L.; Yamauchi, Y.; Guan, B. Y. Hard" Emulsion-Induced Interface Super-Assembly: A General Strategy for Two-Dimensional Hierarchically Porous Metal-Organic Framework Nanoarchitectures. *J. Am. Chem. Soc.* **2024**, *146*, 18979−18988.
(37) Zhou, Z.; Wang, J.; Hou, S.; Mukherjee, S.; Fischer, R. A. Room Temperature Synthesis Mediated Porphyrinic NanoMOF Enables Benchmark Electrochemical Biosensing. *Small* **2023**, *19* (37), 2301933.
(38) Destefano, M. R.; Islamoglu, T.; Garibay, S. J.; Hupp, J. L.; Farha, O. K. Room-Temperature Synthesis of UiO-66 and Thermal Modulation of Densities of Defect Sites. *Chem. Mater.* **2017**, *29*, 1357−1361.
(39) He, H. H.; Li, L. Y.; Liu, Y.; Kassymova, M.; Li, D. D.; Zhang, L. L.; Jiang, H.-L. Rapid Room-Temperature Synthesis of a Porphyrinic MOF for Encapsulating Metal Nanoparticles. *Nano Res.* **2021**, *14*, 444−449.
(40) Zaremba, O.; Andreo, J.; Wuttke, S. The Chemistry Behind Room Temperature Synthesis of Hafnium and Cerium UiO-66 Derivatives. *Inorg. Chem. Front.* **2022**, *9*, 5210−5216.
(41) Li, Y. C.; Su, J.; Zhao, Y.; Feng, L.; Gao, L.; Xu, X. Y.; Yin, Y.; Liu, Y. F.; Xiao, P. W.; Yuan, L.; Qin, J.-S.; Wang, Y. Y.; Yuan, S.; Zheng, H.; Zuo, J.-L. Dynamic Bond-Directed Synthesis of Stable Mesoporous Metal-Organic Frameworks under Room Temperature. *J. Am. Chem. Soc.* **2023**, *145*, 10227−10235.
(42) Benseghir, Y.; Lemarchand, A.; Duguet, M.; Mialane, P.; Gomez-Mingot, M.; Roch-Marchal, C.; Pino, T.; Ha-Thi, M.-H.; Haouas, M.; Fontecave, M.; Dolbecq, A.; Sassoye, C.; Mellot-Draznieks, C. Co-Immobilization of a Rh Catalyst and a Keggin Polyoxometalate in the UiO-67 Zr-Based Metal-Organic Framework: in Depth Structural Characterization and Photocatalytic Properties for CO_2 Reduction. *J. Am. Chem. Soc.* **2020**, *142*, 9428−9438.
(43) Vahabi, A. H.; Norouzi, F.; Sheibani, E.; Rahimi-Nasrabadi, M. Functionalized Zr-UiO-67 Metal-Organic Frameworks: Structural Landscape and Application. *Coord. Chem. Rev.* **2021**, *445*, 214050.
(44) Zhu, Q.; Luo, Y.; Liang, H.; Song, Y.; Ma, G. A Sensitive Electrochemical Biosensor for Detection of Carbaryl Based on Hollow Covalent-Organic Frameworks-Gold Nanoparticles Nanospheres. *J. Environ. Chem. Eng.* **2024**, *12* (3), 112681.
(45) Wang, Y.; Zhao, Q.; Xue, Y.; Wu, D.; Zhang, B.; Sun, J.; Yang, X. Protein-Inorganic Hybrid Nanoflowers with Laccase-Like Activity for Specific Assay of Acetylcholinesterase Activity. *Sens. Actuators, B* **2023**, *396*, 134565.
(46) Li, M. N.; Xie, Y. F.; Lei, L. L.; Huang, H.; Li, Y. X. Colorimetric Logic Gate for Protamine and Trypsin Based on the Bpy-Cu Nanozyme with Laccase-Like Activity. *Sens. Actuators, B* **2022**, *357*, 131429.
(47) Estes, S.-L.; Antonio, M.-R.; Soderholm, L. Tetravalent Ce in the Nitrate-Decorated Hexanuclear Cluster $[Ce_6(\mu_3\text{-}O)_4(\mu 3\text{ }OH)_4]^{12+}$: a Structural End Point for Ceria Nanoparticles. *J. Phys. Chem. C* **2016**, *120*, 5810−5818.
(48) Karmakar, S.; Barman, S.; Rahimi, F. A.; Biswas, S.; Nath, S.; Maji, T. K. Developing Post-Modified Ce-MOF as a Photocatalyst: A Detail Mechanistic Insight into CO_2 Reduction Toward Selective C2 Product Formation. *Energy Environ. Sci.* **2023**, *16*, 2187−2198.
(49) Shearer, G. S.; Chavan, S.; Bordiga, S.; Svelle, S.; Olsbye, U.; Lillerud, K. P. Defect Engineering: Tuning the Porosity and Composition of the Metal-Organic Framework UiO-66 via Modulated Synthesis. *Chem. Mater.* **2016**, *28*, 3749−3761.
(50) Schmidt-Winkel, P.; Lukens, W. W.; Zhao, D.; Yang, P.; Chmelka, B.; Stucky, G. D. Mesocellular Siliceous Foams with Uniformly Sized Cells and Windows. *J. Am. Chem. Soc.* **1999**, *121* (1), 254−255.
(51) Li, K.; Yang, J.; Gu, J. Salting-in Species Induced Self-Assembly of Stable MOFs. *Chem. Sci.* **2019**, *10*, 5743−5748.
(52) Wang, C.; Yan, J.; Chen, S.; Liu, Y. High-Valence Metal-Organic Framework Materials Constructed from Metal-Oxo Clusters: Opportunities and Challenges. *ChemPluschem* **2023**, *88* (3), No. e202200462.
(53) Chen, X.; Zhuang, Y. H.; Rampal, N.; Hewitt, R.; Divitini, G.; O'Keefe, C. A.; Liu, X. W.; Whitaker, D. J.; Wills, J. W.; Jugdaohsingh, R.; Powell, J. J.; Yu, H.; Grey, C. P.; Scherman, O. A.; Fairen-Jimenez, D. Formulation of Metal-Organic Framework-Based Drug Carriers by Controlled Coordination of Methoxy PEG Phosphate: Boosting Colloidal Stability and Redispersibility. *J. Am. Chem. Soc.* **2021**, *143*, 13557−13572.
(54) Jiang, D.; Huang, C.; Zhu, J.; Wang, P.; Liu, Z.; Fang, D. Classification and Role of Modulators on Crystal Engineering of Metal Organic Frameworks (MOFs). *Coord. Chem. Rev.* **2021**, *444*, 214064.
(55) Yao, N.; Jia, H. N.; Zhu, J.; Shi, Z. P.; Cong, H. J.; Ge, J. J.; Luo, W. Atomically Dispersed Ru Oxide Catalyst with Lattice Oxygen Participation for Efficient Acidic Water Oxidation. *Chem* **2023**, *9*, 1882−1896.

https://doi.org/10.1021/jacsau.4c00866
JACS Au 2025, 5, 178−186

(56) Fang, G.; Kang, R. N.; Chong, Y.; Wang, L. M.; Wu, C. Q.; Ge, C. C. MOF-Based DNA Hydrolases Optimized by Atom Engineering for the Removal of Antibiotic-Resistant Genes from Aquatic Environment. *Appl. Catal., B* **2023**, *320*, 121931.
(57) Xu, S.; Wu, H.; Liu, S.; Du, P. D.; Wang, H.; Yang, H.; Xu, W.; Chen, S.; Song, L.; Li, J.; Shi, X.; Wang, Z.-G. A Supramolecular Metalloenzyme Possessing Robust Oxidase-Mimetic Catalytic Function. *Nat. Commun.* **2023**, *14* (1), 4040.
(58) Zhou, G.; Wang, B.; Cao, R. Acid Catalysis in Confined Channels of Metal−Organic Frameworks: Boosting Orthoformate Hydrolysis in Basic Solutions. *J. Am. Chem. Soc.* **2020**, *142* (35), 14848−14853.
(59) Li, T.; Wang, Y.; Liu, W.; Fei, H.; Guo, C.; Wei, H. Nanoconfinement-Guided Construction of Nanozymes for Determining H_2O_2 Produced by Sonication. *Angew. Chem. Int. Ed.* **2023**, *62* (12), No. e202212438.
(60) Sussman, J. L.; Harel, M.; Frolow, F.; Oefner, C.; Goldman, A.; Toker, L.; Silman, I. Atomic Structure of Acetylcholinesterase from Torpedo Californica: A Prototypic Acetylcholine-Binding Protein. *Science* **1991**, *253*, 872−879.

https://doi.org/10.1021/jacsau.4c00866
JACS Au 2025, 5, 178−186